Observation-based estimates of Eulerian-mean boundary downwelling in the western subpolar North Atlantic

Y. J. Liu[1*], D. G. Desbruyères[1], H. Mercier[2] and M. A. Spall[3]

[1]Ifremer, Laboratoire d'Océanographie Physique et Spatiale, UMR 6523 CNRS-IFREMER-IRD-UBO, Plouzané, France

[2]CNRS, Laboratoire d'Océanographie Physique et Spatiale, UMR 6523 CNRS-IFREMER-IRD-UBO, Plouzané, France

[3]Woods Hole Oceanographic Institution, Woods Hole, MA, USA

Contents of this file

> Text S1 to S4
> Figures S1 to S7
> Tables S1

Introduction

The supporting information provides the spatial distribution of the three datasets (ISAS, EN4 and CORA, in Text S1), an evaluation of our specifically-designed OI product (in Text S2), additional details of the transport estimations derived from the three datasets (in Text S3) and the relative importance of temperature and salinity in along-boundary density change (Text S4).

Text S1. Spatial distribution of the data

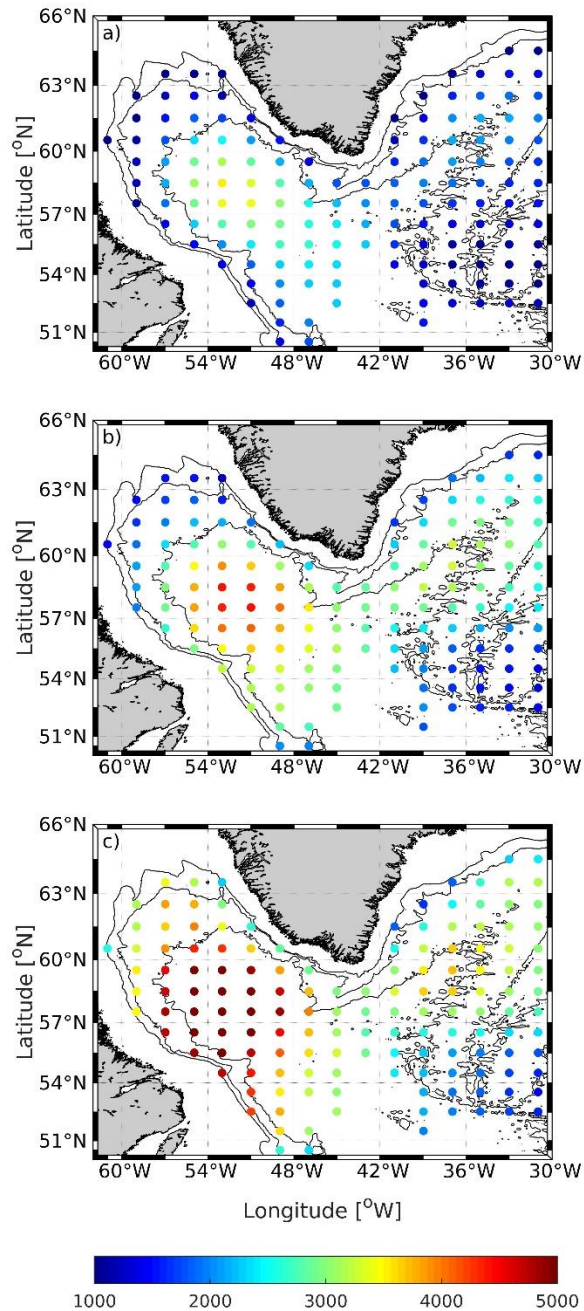Figure S1 illustrates the number of profiles in the research domain.

Figure S1. The number of profiles in each computational box (7.2°× 3.6°) derived from ISAS/CORA/EN4 (a/b/c) datasets between 2002 and 2015. Contours indicate isobaths 1000 m, 2000 m and 3000 m. All three datasets have an irregular and uneven distribution of profiles: the density distribution is largest in the region with a depth of more than 3000 m and decreases toward the shelf. The ISAS dataset contains 600-3000 profiles in each bin. The CORA dataset contains 1000–4000 profiles and the EN4 dataset contains 1000–6000 profiles in each bin.

2

Text S2. Comparison between OI and hydrographic sections

To assess the robustness of our specifically-designed OI product, we compare our estimation to two hydrographic sections, A25-OVIDE and AR7W (see Figure 2 in the paper for the position of the sections). Figures S2 and S3 show summer mean temperature and salinity fields along the OVIDE and AR7W sections. We examine the temperature and salinity profiles of stations along the slope shallower than 3000 m of the OVIDE section (Figure S4(a)(b)(c)) and the AR7W section (Figure S4(d)(e)(f)/Figure S4(g)(h)(i)), respectively. The OI error matrix (used for bootstrap) is compared to the errors between OVIDE/AR7W and OI, at the stations with water depth of 2400 m in Figure S5. Figure S6 shows the overall streamfunctions derived from the three datasets. These intercomparison and error analysis demonstrate that OI-derived fields can be used to describe ocean circulation in both boundary and open-ocean interior basins with satisfactory accuracy.
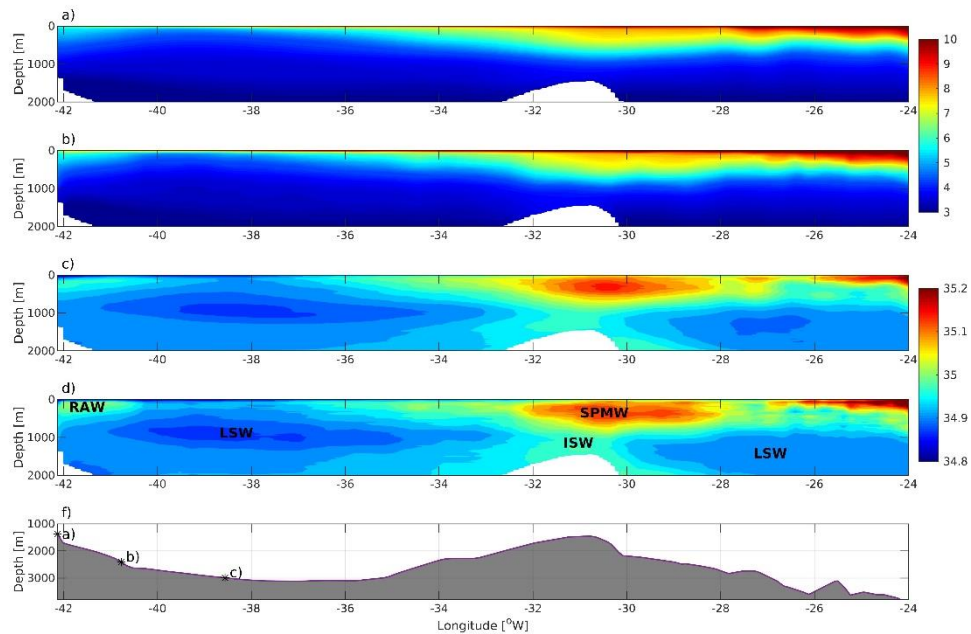

Figure S2. The summer mean potential temperature (°C) and salinity derived from the OI method based on ISAS dataset (a,c) and OVIDE hydrographic data (b,d) along the OVIDE section (see Figure 1). The corresponding bathymetry is shown in (f). The symbol stars in (f) indicate the stations of the profiles in Figure S4. The estimated properties at the OVIDE section based on OI exhibit remarkable consistency with those derived from the shipboard database, such as the slope of isopycnals and the main water masses (such as Recirculating Atlantic Water, Labrador Sea Water, Subpolar Mode Water, and Icelandic Slope Water). The smoother contours and fewer small structures suggest that the data processed by OI tends to filter out undesired high-frequency variability.
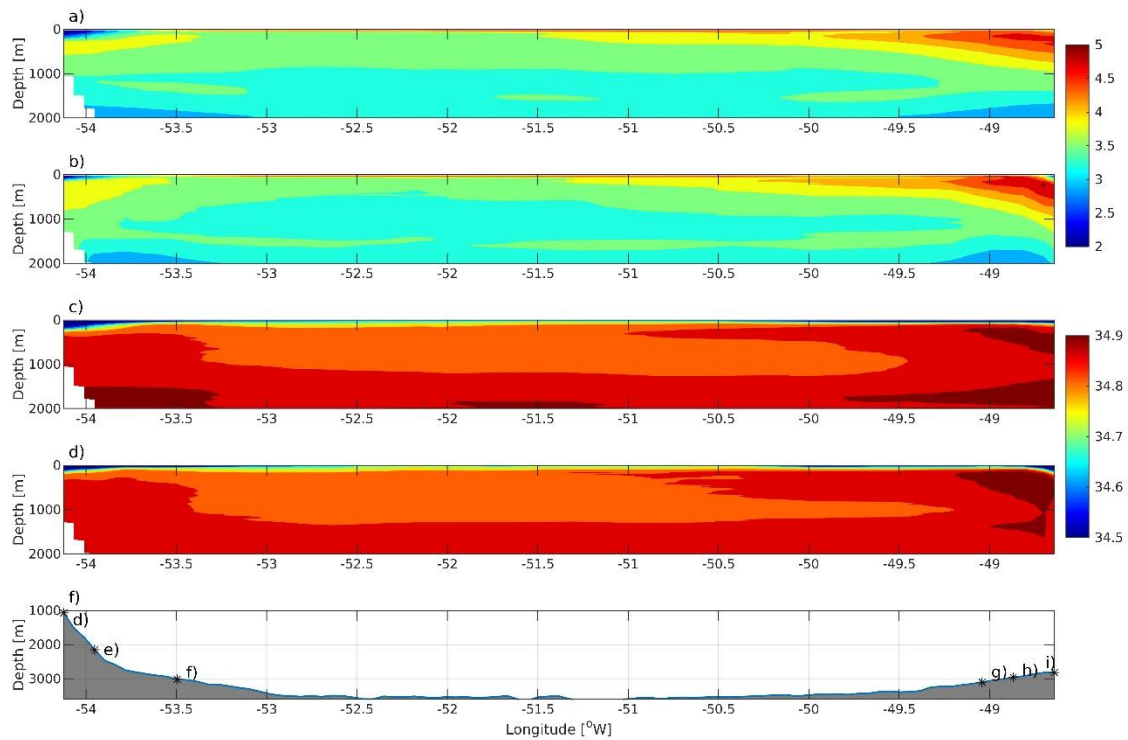
Figure S3. The summer mean potential temperature (°C) and salinity derived from the OI method based on ISAS dataset (a,c) and AR7W hydrographic data (b,d) along the AR7W section (see Figure 1.). The corresponding bathymetry is shown in (f). The symbol stars in (f) indicate the stations of the profiles in Figure S4. The temperature and salinity derived from OI are consistent with the AR7W section profiles. The Labrador Sea Water is evident in the basin's interior as a body of cold, fresh water in the water column's middle (relative to the boundaries). The warm and salty Irminger current transports Irminger water onto the basin's eastern continental slope.
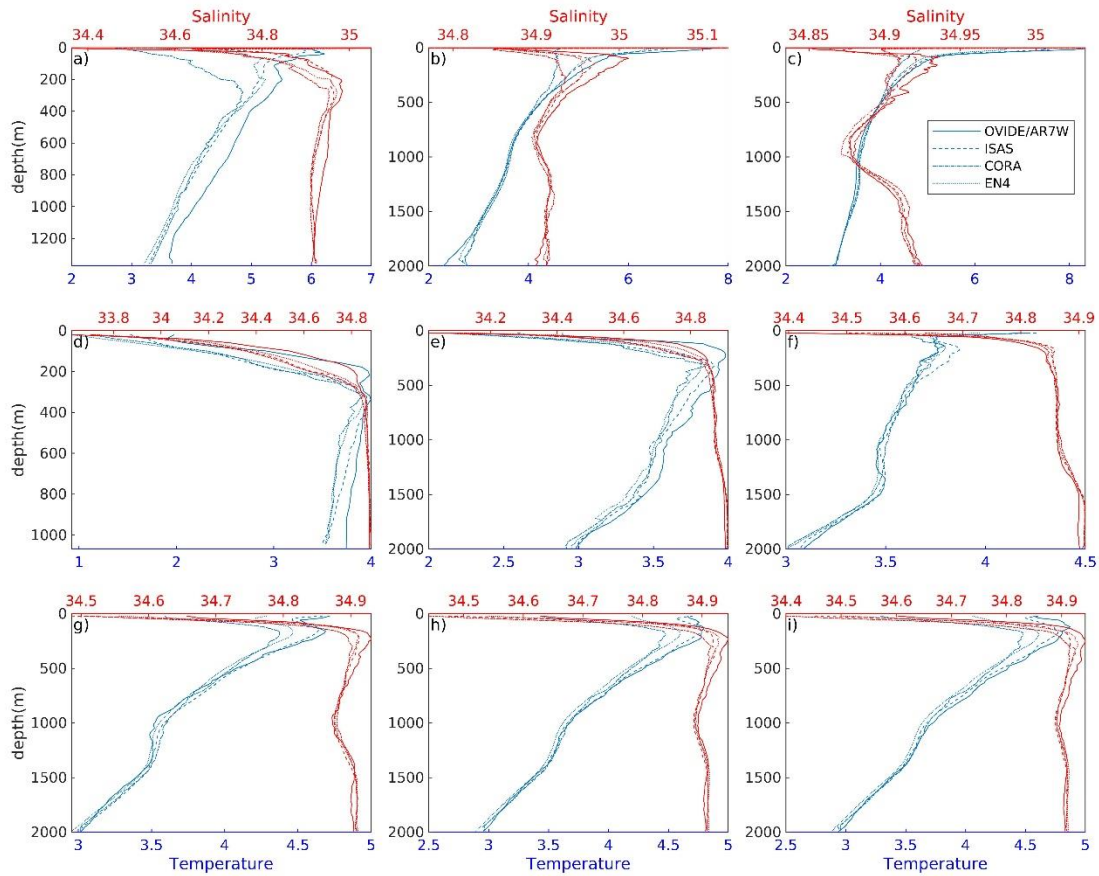
Figure S4. The temperature (blue curves, in °C) and salinity (red curves) profiles from the estimations of OI (dashed lines: dashed-ISAS, dotted dashed-CORA, dotted-EN4) and hydrographic lines OVIDE/AR7W (solid lines) at the stations shown in Figure S2 and Figure S3. The temperature and salinity estimations from the OI agree well with the hydrographic sections. Commonly, significant deviations occur near the sea surface (150 m) due to higher-frequency variations in properties such as freshwater flux and air-sea flux. Nonetheless, the significant surface errors, which account for less than 10% of the water column, will have a negligible effect on the subsequent calculation of the large-scale overturning transport.
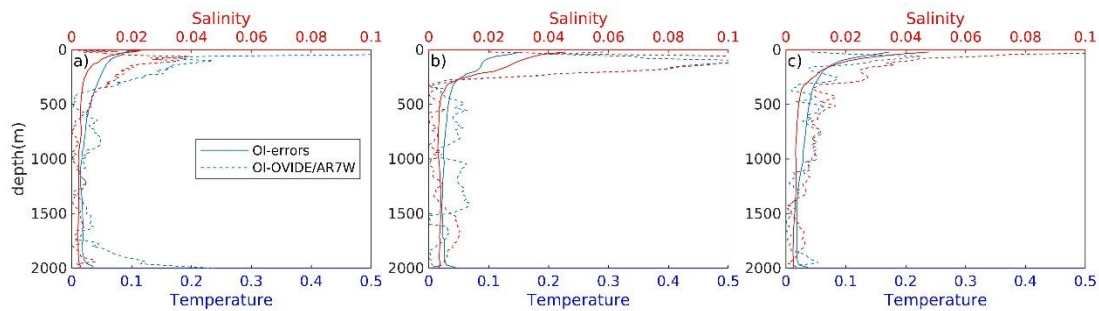

Figure S5. The multi-product mean errors of temperature (blue curves, in °C) and salinity (red curves) from the error matrix of OI used for bootstrap (OI-errors, solid lines) and the errors between OVIDE/AR7W and OI (dashed lines, OI-OVIDE/AR7W) at the stations

5

with water depth of 2400 m (stations b), e), i) in Figure S2 and Figure S3). The OI-OVIDE/AR7W errors are of similar magnitude than the OI-errors, which provides confidence in the bootstrap-based estimations of transport uncertainties along isobath 2400 m.
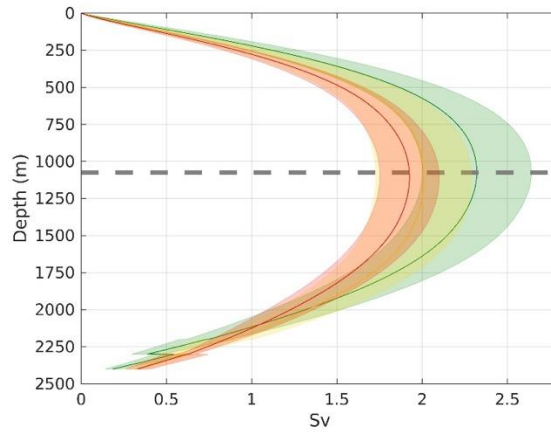

Figure S6. The geostrophic streamfunctions from each product (green-ISAS, gold-CORA, red-EN4) for the whole SPG, as obtained by accumulating the vertical transport from the surface in depth space. The errors in patches are two times of standard deviation derived (STD) from the bootstrap simulations of each product. The dashed line indicates the depth of maximum overturning.

Text S3. The vertical transport in SPG from different datasets and the multiproduct mean

The first three classified rows of Table S1 provide additional information about the Eulerian-mean vertical transport in various regions and seasons as derived from the three individual datasets. Depending on the considered datasets, transport varies slightly and exhibits distinct seasonality in each region. The most notable difference between CORA and ISAS/EN4 is the relatively substantial winter transport in the Labrador Sea in CORA (both downwelling and upwelling regions). The explanation for this substantial downwelling/upwelling is the presence of anomalously light waters (warm and salty) along Greenland's west coast (between s~0.48 and s~0.54 in Figure 2), where the CORA dataset contains more warm and salty profiles. Therefore, the winter transport derived from the CORA dataset is not considered in the transport calculation shown in Figure 4 and Table 1. Our estimations do not yield a conclusive seasonal signature (both along the whole SPG and within individual basins), as no consistent seasonal patterns are observed amongst individual product estimates.

Table S1. The maximum vertical transport (Sv) derived from each product in the three regions (defined in Figure 2) and whole SPG. The errors are two times of standard deviation derived from the bootstrap simulations.

Dataset	Season	LD	LU	ID	SPG

	Winter	2.06±0.21	-2.54±0.24	2.54±0.29	2.06±0.38
	Spring	2.38±0.28	-1.92±0.22	2.15±0.28	2.61±0.41
ISAS	Summer	2.32±0.14	-1.84±0.21	2.11±0.28	2.58±0.35
	Autumn	2.86±0.13	-2.62±0.18	2.07±0.28	2.31±0.35
	Annual	2.40±0.75	-2.23±0.88	2.22±0.48	2.39±0.32
	Winter	**3.35±0.17**	**-3.33±0.20**	2.51±0.32	2.53±0.38
	Spring	2.22±0.26	-2.00±0.19	1.52±0.22	1.74±0.36
CORA	Summer	2.10±0.15	-1.84±0.17	1.63±0.18	1.89±0.26
	Autumn	2.25±0.13	-1.94±0.16	1.83±0.26	2.15±0.33
	Annual	2.48±1.15	-2.27±1.36	1.87±0.81	2.08±0.28
	Winter	1.88±0.11	-2.57±0.12	2.67±0.24	1.98±0.26
	Spring	2.21±0.20	-2.21±0.12	2.10±0.13	2.09±0.24
EN4	Summer	2.06±0.09	-1.73±0.10	1.77±0.08	2.10±0.13
	Autumn	2.50±0.08	-2.26±0.13	1.72±0.21	1.96±0.24
	Annual	2.16±0.56	-2.19±0.69	2.07±0.93	2.03±0.18

Text S4. The relative importance of temperature and salinity in boundary downwelling

We simply decompose the density change using a linear equation of state:

$$\frac{\rho - \rho_0}{\rho_0} = -\alpha(T - T_0) + \beta(S - S_0) \qquad (S1)$$

The α and β are the thermal expansion and saline contraction coefficients, respectively, which are determined by temperature and salinity. To investigate the downstream density variation starts from DKS (s=0), ρ_0, T_0 and S_0 are assumed to be the values at s=0 of isobath 2400 m. The terms in the rhs of the equation $-\alpha(T - T_0)$, $\beta(S - S_0)$ then indicate their relative importance in determining the density change $(\rho - \rho_0)/\rho_0$ along the boundary. The three components along the SPG in the upper layer (above 300m) and in the intermediate layer (300-1500m) are presented in Figure S7.
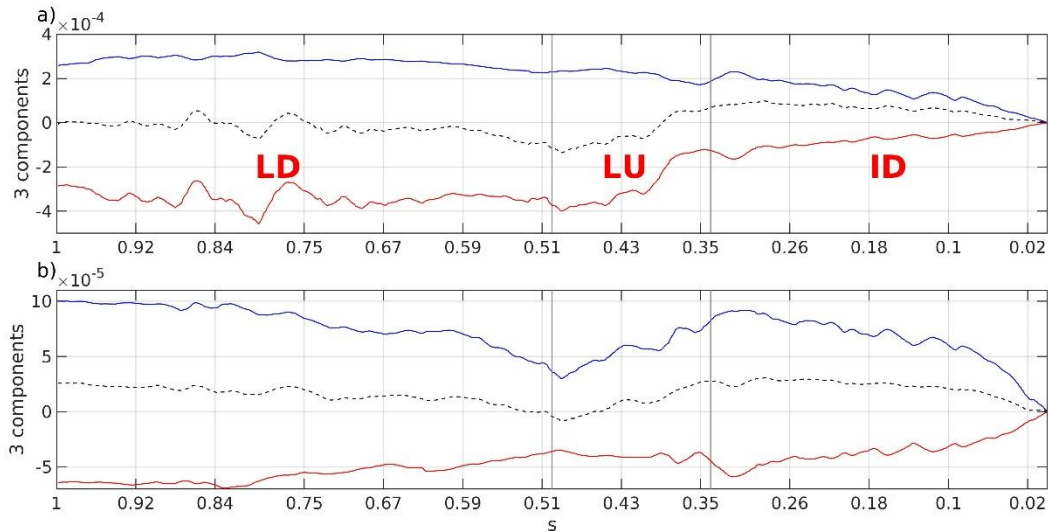
Figure S7. The three terms in equation S1, i.e., density component (dashed black curve), temperature component (solid blue curve), and salinity component (solid red curve) along the boundary from s=0 to s=1 averaged in the upper layer (1-300 m, panel a) and in the intermediate layer (301-1500 m, panel b), for the three distinct regions defined in Figure 1. Temperature and salinity play opposing roles in the along-boundary density variation. In the upper layer, the along-boundary density change is significantly contributed by temperature in the Irminger Sea (ID) and by salinity in the Labrador Sea (LD and LU); in the intermediate layer, the density change is overly determined by temperature. As the overall density change in the upper layer is negligible and the significant along-boundary density gradient occurs in the depth of around 1000 m, the Eulerian boundary transport is mostly a result of boundary cooling in the intermediate layers.
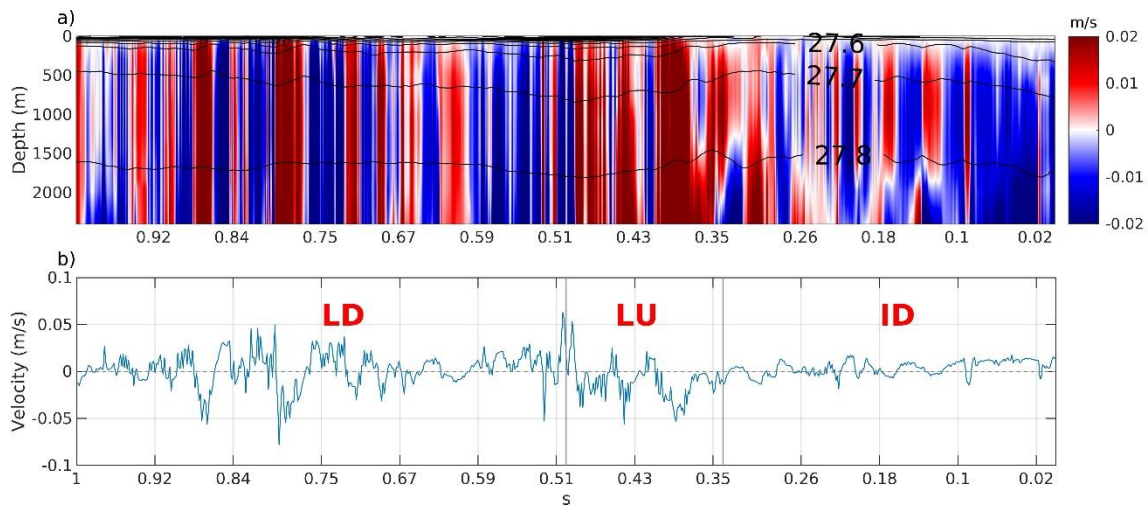

Figure S8. The baroclinic (panel(a)) and reference (panel(b)) velocities fields in equation 2 along isobath 2400 m. The positive (negative) values indicate inshore (offshore) flows.